International Journal of Heat and Mass Transfer 52 (2009) 1741–1752

Contents lists available at ScienceDirect

International Journal of Heat and Mass Transfer

journal homepage: www.elsevier.com/locate/ijhmt

Measurement of flow maldistribution in parallel channels and its application to ex-situ and in-situ experiments in PEMFC water management studies

S.G. Kandlikar *, Z. Lu, W.E. Domigan, A.D. White, M.W. Benedict

Thermal Analysis, Microfluidics, and Fuel Cell Laboratory, Rochester Institute of Technology, 76 Lomb Memorial Dr., Rochester, NY 14623, USA

ARTICLE INFO

Article history:
Received 6 June 2008
Received in revised form 22 September 2008
Available online 29 November 2008

Keywords:
Maldistribution
PEM fuel cell
Gas channels
Instantaneous channel flow rates

ABSTRACT

Uniform flow distribution is critical to obtaining high performance in many heat and mass transfer devices. It also plays an important role in the effective operation of a proton exchange membrane fuel cell (PEMFC). Presently there are a few theoretically based models available for predicting flow distribution in individual fuel cell channels and across fuel cell stacks in PEMFCs, but little or no experimental data has been published on the actual flow rates measured in individual channels. This is mainly because of the lack of experimental techniques available to measure the instantaneous flow rates in parallel channels. In this work, a novel technique based on the entrance region pressure drop measurements is presented for monitoring fluid flow maldistribution in individual channels. The method is validated using liquid water flow in a test section with four tubes in parallel, and then applied to assess the air flow maldistribution in PEMFCs using (a) an ex-situ experimental setup simulating the two-phase flow in parallel channels, and (b) an in-situ experimental setup with an operating fuel cell. While an almost uniform air distribution is obtained for the parallel channels with an impermeable backing (plastic sheet), severe maldistribution is observed for the same channels with porous GDL backing. The maldistribution caused by the water blockage in an ex-situ test setup is further investigated and the results are verified by the high-speed images of the two-phase flow in channels. The technique has also been applied in an in-situ experimental setup to obtain the flow maldistribution under electrochemical reaction conditions in the presence of two-phase flow in the cathode side gas channels.

1. Introduction

Fluid flow devices often employ multiple parallel channels, for example, to enhance heat transfer in heat exchangers, enhance mass transfer in absorbers, or improve fluid transport and distribution in fuel cell gas channels. The smaller channels provide increased surface area, while the inlet and exit manifolds facilitate necessary distribution and provide connections to external inlet and outlet conduits. Flow maldistribution in heat exchangers has been studied by a number of researchers. Non-uniform flow in channels leads to different performance penalties depending on the process. For example, gross flow maldistribution leads to significant reduction in effectiveness for high NTU heat exchangers [1], about 7% for condensers, and up to 25% for cross-flow exchangers [2]. Mueller and Chiou [1] list various factors responsible for flow maldistribution in a shell and tube heat exchanger: entry problems due to header design, bypass streams and fabrication tolerances. Kitto and Robertson [3] provide a good summary of maldistribution in heat exchangers and indicate that the problem is more severe in two-phase devices, such as evaporators, condensers, absorbers, reboilers, etc.

In general, maldistribution in parallel channels is caused by:

(a) Uneven local pressure distribution in the inlet/exit manifolds apparent at the channel entrance/exit, caused by the specific placement of the inlet/outlet pipes, fluid distribution in the headers, buoyancy effects, two-phase separation and resultant flow non-uniformity.
(b) Uneven flow resistances in the parallel channels caused by variations in channel dimensions, different flow lengths, uneven fouling, density and viscosity variations, and presence of two or more phases.

Lalot et al. [2] identified that the kinetic energy of the fluid brought in by the inlet pipe into the inlet manifold causes local pressure variations at the entrance to the channels. The local pressure distribution at the face of the channels is affected by the local velocity distribution. If the inlet pipe is facing the channel entrance, then the pressure in the area immediately facing the pipe has an

* Corresponding author. Tel.: +1 585 475 6728; fax: +1 585 475 7710.
E-mail addresses: sgkeme@rit.edu (S.G. Kandlikar), zxleme@rit.edu (Z. Lu), wed8908@rit.edu (W.E. Domigan), adw2888@rit.edu (A.D. White), mwb4959@rit.edu (M.W. Benedict).

0017-9310/$ - see front matter © 2008 Elsevier Ltd. All rights reserved.
doi:10.1016/j.ijheatmasstransfer.2008.09.025

Nomenclature

A	tube extension, 23-mm length	PEM	proton exchange membrane
A_c	cross-sectional area, m^2	PEMFC	proton exchange membrane fuel cell
B	tube extension, 34 mm length	Re	dimensionless Reynolds number
CFD	computational fluid dynamics	u_m	average velocity, m/s
D_h	hydraulic diameter, m	x	entrance length, m
K	modified coefficient	x^+	dimensionless hydrodynamic entry length
K_c	contraction loss coefficient	ρ	density, kg/m^3
MEA	membrane electrode assembly	Δp	differential pressure drop, Pa

additional pressure head of $\frac{1}{2}\rho v^2$ due to the inlet velocity V. The local velocity vectors at the entrance to each channel determine this additional head, which could result in a reverse flow in the channels under extreme conditions.

Plate heat exchangers have been investigated extensively for the pressure variations in the inlet ports and its implication in flow maldistribution and performance degradation. Tereda et al. [4] measured the pressure distribution inside the port and individual channels of a plate heat exchanger to estimate the flow rates in different channels without disturbing the flow. Bobbill et al. [5] developed a generalized mathematical model to study the effect of flow maldistribution on the condensation in a plate heat exchanger. Bobbill et al. [6] measured the port to channel pressure drop by introducing pressure probes. Their results indicate that the flow maldistribution increases with increase in the overall pressure drop. Li et al. [7] used the particle image velocimetry (PIV) technique to investigate the flow characteristics of the flow field in the entrance region of a plate-fin heat exchanger. Rao et al. [8] conducted experimental and theoretical study to show that the performance of a heat exchanger was affected by the port-to-channel flow maldistribution in single-pass and multipass heat exchangers. The maldistribution reduced with multipassing. The effect of the manifold was investigated analytically by Baek and Jiao [9]. They found that optimizing the distributor configuration greatly reduced the flow maldistribution. Rao and Das [10] confirmed the validity of their analytical techniques that showed that the pressure drop increases with the presence of flow maldistribution in a plate heat exchanger. Zhang et al. [11] and Jiao et al. [12,13] experimentally studied the flow maldistribution caused by the defects in the inlet configuration and emphasized the need for proper distributor design.

Gas channels in a PEMFC experience two-phase flow, which is one of the main reasons for flow maldistribution. The effects of flow maldistribution may be quite serious in gas channels of a fuel cell, as it leads to non-uniform current density, localized hot spots in the membrane, performance degradation, and material degradation. Although the problem has been addressed largely through numerical simulation, experimental data and an insight into the factors responsible for maldistribution continues to be an area of intense current interest.

A uniform distribution of current density is of paramount importance for fuel cell operation; it leads to uniform distribution of temperature and liquid water production, and lower mechanical stresses on the membrane electrode assembly (MEA) [14]. The current density distribution in a PEMFC is determined by the uniformity of the reactant gas supply over the catalyst layer. Flow maldistribution is also an important factor in reducing the operating life of a fuel cell [15,16]. Proper reactant distribution is therefore critical to ensure high performance and long lifetime of a PEMFC.

Flow field design and header configuration significantly affect the flow non-uniformity. Various complex flow fields, such as serpentine channels, multiple parallel channels and interdigitated channels, have been investigated for flow maldistribution in PEM fuel cells. Dutta et al. [17,18] examined the performance of straight and serpentine channels. Jen et al. [19] predicted the cell performance with straight channels. Kumar and Reddy [20] examined the impact of channel dimensions and shape for serpentine flow fields on cell performance and later for porous metal foams [21]. They observed a more uniform current density distribution with metal foam compared to a multi-parallel channel flow field design. Senn and Poulikakos [22] and Hontanon et al. [23] also found that porous materials yielded better flow distributions and improved mass transfer, and consequently higher cell performance compared to grooved straight and serpentine flow channels. Barreras et al. [24,25] implemented flow visualization by the laser-induced fluorescence as well as measurements of the velocity field by dye trace tracking to study the flow distribution in a parallel diagonal channel, a branching cascade type, and a serpentine-parallel flow topology. They found that very homogeneous velocity and pressure fields are obtained for both the serpentine-parallel and the cascade-type flow topologies, while an uneven flow distribution was obtained with the diagonal topology. Um and Wang [26] and Hu et al. [27] compared the interdigitated flow channels with parallel straight channels and reported that an interdigitated flow channel could enhance mass transport and improve the PEMFC performance compared to a parallel channel due to forced convectional flow through the porous diffusion layer. Birgersson and Vynnycky [28] numerically simulated and quantitatively compared the performance of the interdigitated channels, parallel channels, and porous foam, and concluded that the foam yielded the most uniform current density distribution and the interdigitated channels can sustain the highest current densities. The advantage and disadvantage of some of the flow-fields have been discussed in several reviews [29,30].

At the stack level, flow maldistribution is more severe due to the multi-duct (individual cells are sometimes referred to as ducts) configuration. However, due to the complexity of the problem and the lack of an experimental technique to measure the instantaneous flow distribution, very few investigations have been reported for the stack level maldistribution. Ganesh et al. [31] mathematically defined a flow maldistribution parameter in terms of the duct inlet velocity and numerically simulated the flow distribution in a PEMFC stack by using flow channeling theory and found a considerably skewed flow distribution which is dominated by flow rate and port size. Bansode et al. [32] carried out a 3D numerical single-phase study to analyze the flow maldistribution in a PEMFC stack with four ducts. Their results showed that the variation in port diameter leads to different degrees of maldistribution and the corresponding non-uniform water content in the membrane. Koh et al. [33] reported a numerical model to investigate pressure variation and flow distribution of stacks. Chen et al. [34] constructed a 2D stack model composed of 72 cells filled with a porous medium to evaluate pressure variation and flow distribution in the manifold of a fuel cell stack. Their modeling results indicated that although both the channel resistance and the manifold

width can enhance the uniformity of the flow distribution, larger manifold width is a better solution for flow distribution because increasing the channel resistance requires an excessive pressure drop which is not beneficial in practical applications.

Similar to the results obtained for heat exchangers [3], the flow maldistribution is induced not only by the cell design but also by local water blockage in the channels. Water accumulation (resulting from vapor condensation and/or product water) in the catalyst layer, GDL, and in gas channels will fill the pores from micro- to macro-sizes and block the gas pathways. This is the well-known flooding phenomenon which can cause major problems with gas distribution and consequently damage the cathode catalyst layers [35]. Presence of water in the individual channels leads to different two-phase flow patterns that affect the gas flow rates in those channels as well as in the other parallel channels due to cross-communication between the channels through the manifolds. An important objective of this work is to identify the flow maldistribution caused by the presence of water in the channels and investigate the flow interaction between adjacent channels.

Flow distribution studies in PEMFCs were primarily limited to flow fields without considering the effect of the gas diffusion layer. In a PEMFC the flow fields are in direct contact with the diffusion layer which helps in distributing the reactants uniformly over the catalyst layer. Consequently, the flow distribution in the flow field needs to be further linked with the flow distribution in the diffusion layer. Dole et al. [36] studied the interaction between the diffusion layer with different permabilities and flow field designs, and concluded that even a meander structure distributes the reactants non-homogeneously on the electrodes due to the additional flow paths available in the diffusion layer. Kanezaki et al. [37] studied the cross-leakage flow between adjacent flow channels in a single channel serpentine flow field and found a significant amount of the cross-leakage flow. This flow is comparable with the flow in the serpentine path due to the pressure gradient set up across the porous diffusion layer between the adjacent channels. Given the considerable influence of the diffusion layer on the flow distribution in PEMFC channels, it becomes relevant to measure the instantaneous flow rate in the channels with a diffusion layer backing rather than in channels with impermeable walls.

This paper is organized as follows: In the first part, a technique for experimentally measuring instantaneous flow rates in individual parallel channels is presented. The technique is validated using a well-defined geometry with four circular tubes with different individual lengths connected in parallel to a common header. In the second part, the technique is implemented in an ex-situ experimental facility that is developed for studying two-phase flow, GDL intrusion, and GDL-channel interactions simulating the water transport in a PEMFC. Finally, in the third part, the technique is applied to an in-situ PEMFC fuel cell test section to study the two-phase flow phenomena in the cathode side gas channels.

2. Theory and validation of the entrance region pressure drop method

In this section, the theory of the entrance region pressure drop is first introduced and validated in a four-tube parallel channel geometry. An experimental test section is designed to validate/modify the theoretical equations using water as the fluid. The experimental test section is then modified to intentionally introduce flow maldistribution. Extension tubes with two different lengths of 34 mm and 23 mm are added to one or two flow tubes. By doing so, the flow resistances in the extended tubes increase and flow rates in them decrease. The flow rate distribution is then predicted from the theoretical equations based on the entrance region pressure drop measurements and compared with actual measurements.

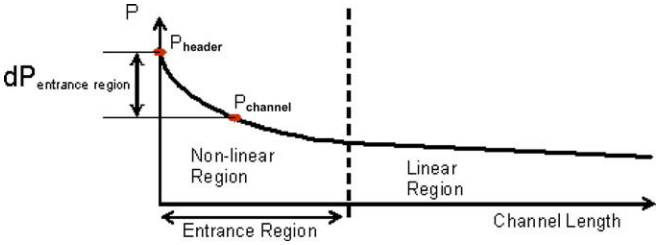

Fig. 1. Variation of pressure as a function of length in a tube or a channel.

2.1. Theoretical work

The equations derived for the developing laminar flow in circular ducts is used to describe the entrance region pressure drop within the tubes. Fig. 1 is a schematic representation of the channel pressure as a function of length. There is a non-linear relationship in the entrance region, beyond which the flow is fully developed and a linear relationship emerges.

The pressure drop in the tube entrance region is the summation of two components: a frictional pressure drop, which accounts for the greatest portion of the total pressure drop, and the minor pressure drop, caused by entrance region effects. An equation for the core pressure drop has been determined by Hornbeck [38] through previous studies. A contraction loss coefficient is used to account for the minor losses.

Eq. (1), obtained by Hornbeck [38], accurately describes the core frictional pressure drop, Δp, in the developing (entrance) region of a circular duct.

$$\frac{\Delta p_{core}}{(1/2)\rho\ u_m^2} = 13.74(x^+)^{1/2} + \frac{1.25 + 64x^+ - 13.74(x^+)^{1/2}}{1 + 0.00021(x^+)^{-2}} \tag{1}$$

where ρ is the fluid density, u_m is the mean fluid velocity in the channel, and the non-dimensionalized length is represented by x^+.

$$x^+ = \frac{x/D_h}{\mathrm{Re}} \tag{2}$$

where x is the distance from the entrance, D_h is the hydraulic diameter, and Re is the Reynolds number. The Reynolds number is a function of the flow rate.

A minor loss coefficient, termed the contraction loss coefficient, K_c, is introduced to account for the entrance losses [39]. Eq. (1) is then replaced by the following equation as the final theoretical relationship for the entrance region pressure drop and the mean flow velocity in the channel.

$$\frac{\Delta p}{(1/2)\rho u_m^2} = K_c + 13.74(x^+)^{1/2} + \frac{1.25 + 64x^+ - 13.74(x^+)^{1/2}}{1 + 0.00021(x^+)^{-2}} \tag{3}$$

where K_c is the contraction coefficient and x^+ is the non-dimensional channel length. From this equation, the mean fluid velocity and hence the mass flow rate in a channel of known hydraulic diameter can be estimated from the measured pressure drops in the entrance region as long as the contraction loss coefficient K_c is known. This coefficient is a function of the channel diameter, manifold diameter and the entrance conditions [39].

Eq. (3) is valid for single phase flow in circular channels in the laminar flow regime. For micro- and mini-channel applications, such as PEMFCs, laminar flow generally exists due to the relatively low flow rates and the small hydraulic diameters. Water is used in the validation experiments because the flow rate can be easily and

accurately measured by collecting the water from individual channel outlets over a known time duration.

The experimental test section is schematically shown in Fig. 2. It comprises of an inlet manifold made of polycarbonate (Lexan®) and four stainless steel tubes of 0.54 mm inner diameters and 82.5 mm length to serve as parallel channels. A common pressure tap hole is made in the manifold from which the total entrance region pressure differential and individual entrance region pressure differentials are measured. Two entrance lengths (defined from the tube entrance to the center of the pressure tap) of 10 mm and 15 mm (confirmed to be in the entrance region for all flow conditions tested) are selected for the pressure drop measurements. The entrance region pressure drops are measured by individually calibrated Omega PX26-001DV differential pressure sensors, which have an accuracy of ±.07 kPa in the range of 0–7 kPa. Deionized water is degassed in order to ensure a single phase flow and is provided to the minitubes via an external gear pump (Micropump GA-V23) and an Omega FLR1001 air/water flow meter. Prior to the measurement of the pressure drops, the degassed water is allowed to run through the test section for at least five minutes to reach the steady state. The Micropump control, flow meter, and pressure sensors are interfaced with LabVIEW. All experiments are conducted with water at a temperature of 24 °C.

In order to check the validity of Eq. (3), calibration testing is carried out where only one tube is left open and others are blocked, and the water flow rate and the pressure drop in the entrance region of the tube are recorded. The measured individual channel flow rate and corresponding pressure drop are summarized in Fig. 3. The pressure drop is also calculated from Eq. (3) with a K_c value of 1.07 as suggested by Kays and London [39]. The pressure drop is calculated using Eq. (3) and compared with the actual reading. Large deviation is found between the theoretical and the measured values especially at higher flow rates, with an average deviation of 12.4%. This discrepancy is attributed to the experimental uncertainties and the specific K_c value from Kays and London. Their value is derived from macro-scale experiments and its applicability to the micro-scale tubes used in the present study is in question. In order to improve the agreement between predicted pressure drops and experimental data in Fig. 3, the value of K_c was actually determined iteratively from Eq. (3) over the full range of flow rates for each tube. It varied between 1.0 to 1.45 over the

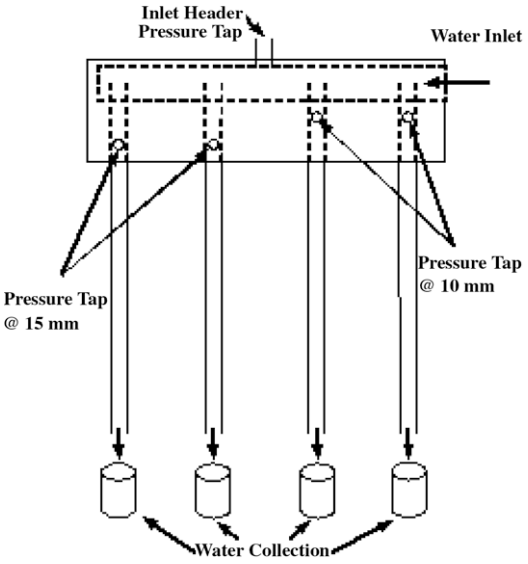

Fig. 2. Schematic of four tube test section used to validate the entrance region pressure drop method. Not to scale.

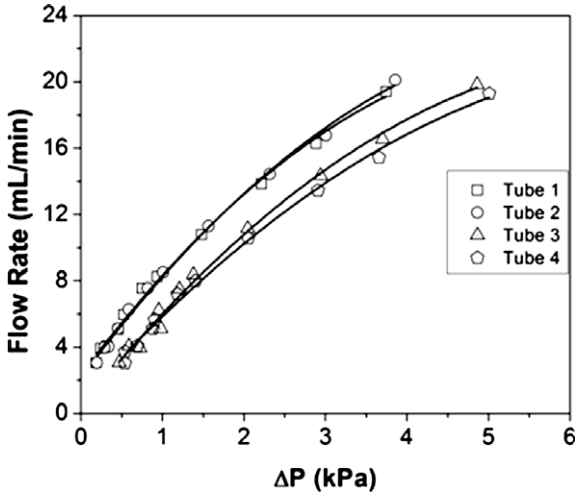

Fig. 3. Baseline flow predictions based on entrance region pressure drop in each tube.

Reynolds number range between 350 and 850. It is found that the new K_c value is a function of Reynolds number rather than a constant. The individual equations for K_c are given by the following equations over the Reynolds number range of $350 \leqslant Re \leqslant 850$:

$$\text{Tube1}: \quad K_c = -0.9247 + 7.236 \times 10^{-3}\text{Re} - 5.301 \times 10^{-6}\text{Re}^2 \quad (4)$$

$$\text{Tube2}: \quad K_c = -0.1404 + 4.454 \times 10^{-3}\text{Re} - 3.192 \times 10^{-6}\text{Re}^2 \quad (5)$$

$$\text{Tube3}: \quad K_c = 1.376 + 1.134 \times 10^{-4}\text{Re} + 1.209 \times 10^{-7}\text{Re}^2 \quad (6)$$

$$\text{Tube4}: \quad K_c = 1.047 + 1.287 \times 10^{-3}\text{Re} - 8.436 \times 10^{-7}\text{Re}^2 \quad (7)$$

The modified K_c values are then substituted back in Eq. (3) to predict the theoretical pressure drop values. The predicted pressure drops are also plotted in Fig. 3 as the respective lines. A good agreement is now obtained between the predicted values and the measured ones, with an average deviation of 7.0% over the entire flow rate range. It is worthy to note that the new K_c values obtained here are specific to the test setup and operating conditions of the present experimental work and may not be used under other experimental conditions. They include the effect of specific header distribution as well. Since these values are seen to differ significantly from the macroscale values from Kays and London [39], it is seen that there is a need for generating the contraction (as well as expansion) coefficients for microscale flows (a range below 3 mm is suggested).

Eq. (3) with new K_c values is then used to predict the flow rates while operated under different parallel channel configurations. The results are presented in the following section.

2.2. Parallel channel validation experiments

Eq. (3) with modified K_c is seen to accurately predict the individual channel flow rate based on the entrance region pressure drop measurements. In this section, the validity of using Eq. (3) to detect the flow maldistribution in parallel channel configuration is investigated. Flow non-uniformity is intentionally induced by adding extension tubes at the exits of a few selected tubes.

Two tube extension lengths of 34 mm (extension A) and 23 mm (extension B) are employed. Single tube extension and combinations of the tube extensions are used to induce flow maldistribution. A summary of all nine cases tested for the single tube extension experiments is listed in Table 1. Table 2 lists the summary of the twelve multiple extension cases. The pressure drop in individual tubes is recorded by LabVIEW. The total water flow rate is monitored by an Omega FLR1001 air/water flow meter

Table 1
Single extension cases tested for validation of the entrance region pressure drop method. (The 34 mm extension is represented by "A" and the 23 mm extension is represented by "B".)

Case #	Tube #			
	1	2	3	4
0	–	–	–	–
1.A	A	–	–	–
1.B	B	–	–	–
2.A	–	A	–	–
2.B	–	B	–	–
3.A	–	–	A	–
3.B	–	–	B	–
4.A	–	–	–	A
4.B	–	–	–	B

Table 2
Multiple extension cases tested for validation of the entrance region pressure drop method. ("A" represents the 34 mm extension and "B" represents the 23 mm extension.)

Case #	Tube #			
	1	2	3	4
1.2	A	B	–	–
1.3	A	–	B	–
1.4	A	–	–	B
2.1	B	A	–	–
2.3	–	A	B	–
2.4	–	A	–	B
3.1	B	–	A	–
3.2	–	B	A	–
3.4	–	–	A	B
4.1	B	–	–	A
4.2	–	B	–	A
4.3	–	–	B	A

before it enters the inlet manifold. The flow rate in each tube is determined by collecting and weighing the water from the tube outlets over a known time-interval after the flow is stabilized.

2.2.1. Single extension experiments

During the single extension experiments, the extension is placed on only one tube. The total flow rate is chosen to be 50 ml/min, which corresponds to an average Reynolds numbers for each tube in the range of 500–525 assuming uniform flow distribution in the four tubes. Fig. 4 displays the flow rate in each tube for case 1.A, as a typical example. From this figure, it is seen that the flow rate through the extended tube (tube 1) is greatly reduced, while the flow increases in all other tubes such that the total flow rate remains constant. This is expected because the extra length in tube 1 results in an increased flow resistance.

The theoretical flow rates in each tube are then calculated by using Eq. (3) with the modified K_c values obtained in Section 2.1. The comparison between the predicted flow rates and the measured ones is also shown in Fig. 4. The agreement is seen to be good, with an average error of about 2.5%. Other arrangements have also been tested and similar results are obtained. All the results for the single extension experiments are summarized in Table 3.

2.2.2. Multiple extension experiments

For the multiple extension experiments, two extensions of lengths 34 mm and 23 mm are placed on two different tubes. As a typical example, Case 1.2 from Table 2, in which the 34 mm extension is placed on tube 1 and the 23 mm extension is placed on tube 2, is discussed in detail here. The measured flow rates in each tube for this case with a total flow rate of 50 mL/min are

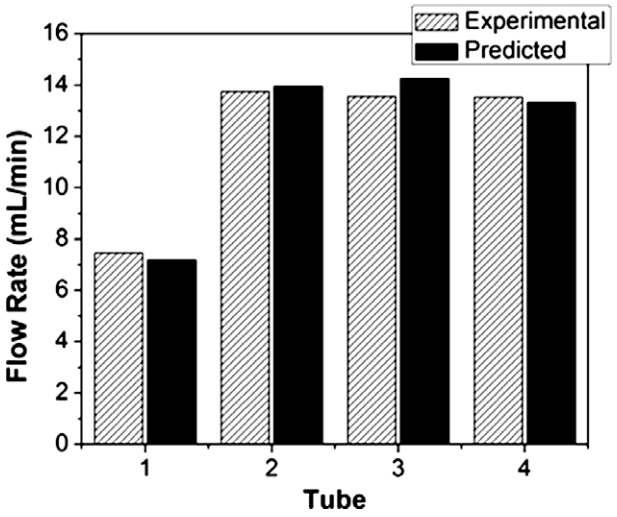

Fig. 4. Results for case 1.A in which tube 1 has the 34 mm extension showing decrease in flow of tube 1; experimental data – measurement of water flow through individual tubes; predicted flow rates determined from Eq. (3).

shown in Fig. 5. As can be seen, the flow rates in tube 1 and 2 are greatly reduced, while the flow rates in tubes 3 and 4 are increased correspondingly. This is again expected due to the increased flow resistance in these two tubes caused by the extra length. It is also noted that that the measured flow rate in tube 1 is a slightly lower than that in tube 2. This is attributed to the longer extension in tube 1, causing greater flow resistance. Likewise, it is also observed that tube 3 shows a slightly higher flow rate than tube 4. This may be due to local pressure variations within the header.

The predicted flow rates from the entrance pressure drop measurements are also plotted in Fig. 5 for comparison. Again, a good agreement is obtained between the predicted and measured flow rates. This indicates that Eq. (3) can be used for detecting the flow maldistribution. Other arrangements have also been tested, and good agreement is consistently obtained between prediction and measurements. An average error of 3.3% is obtained from all multiple extension experiments. Table 4 summarizes all the results for the multiple extension experiments. Error bars are shown in fig-

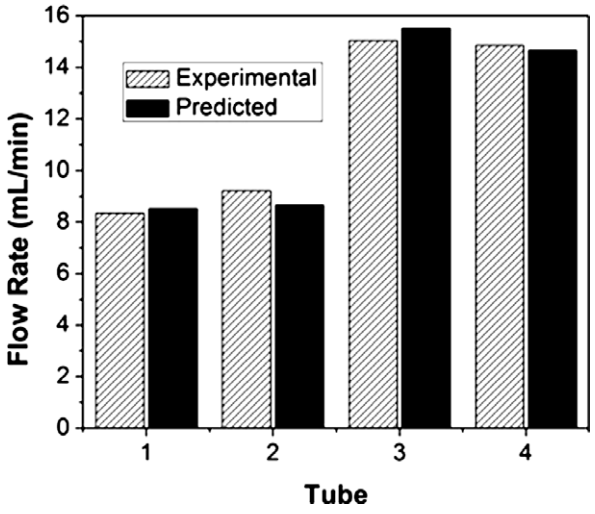

Fig. 5. Results from case 1.2 with the 34 mm extension on tube 1 and the 23 mm extension on tube 2; experimental data – measurement of water flow through individual tubes; predicted flow rates determined from Eq. (3).

Table 3
Summary of case 1.A- 34 mm extension on tube 1. (The difference and the percent difference are between the measured and predicted flow rates. The total is the sum of the tube values, excluding the average.)

Case 1.A	Measured flow rate (mL/min)	Predicted flow rate (mL/min)	Difference (mL/min)	% Difference
Tube 1	7.458	7.188	0.270	3.622
Tube 2	13.752	13.956	0.203	1.478
Tube 3	13.564	14.250	0.685	5.053
Tube 4	13.539	13.332	0.207	1.526
Average	12.078	12.181	0.341	2.920
Total	48.313	48.725	0.412	0.853

Table 4
Summary of case 1.2 with a 34 mm extension on tube 1 and a 23 mm extension on tube 2. (The difference and the percent difference are between the measured and predicted flow rates. The total is the sum of the tube values, excluding the average.)

Case 1.2	Measured flow rate (mL/min)	Predicted flow rate (mL/min)	Difference (mL/min)	% Difference
Tube 1	8.353	8.528	0.175	2.092
Tube 2	9.218	8.665	0.553	5.996
Tube 3	15.052	15.522	0.471	3.126
Tube 4	14.859	14.678	0.181	1.215
Average	11.870	11.848	0.345	3.107
Total	47.481	47.393	0.088	0.185

ures to represent the experimental uncertainties associated with the measurements.

Figs. 4 and 5, along with Tables 3 and 4, demonstrate the effectiveness of the entrance region method in detecting flow distributions across parallel channels. Although water is used as the working fluid, this technique should also be well-suited for detecting gas flow maldistribution. It may be noted that Eq. (3) is applicable here because circular tubes are used. However, in real fuel cell applications, the tubes may be of different shapes, and it may not be possible to accurately predict the contraction coefficient K_c. To overcome this difficulty, a calibration curve may be developed for predicting the individual channel flow rate based on the entrance region pressure drop in that channel. This calibration curve is then used to predict the flow rate from the entrance region pressure drop measurements under parallel channel operation. This approach will be used in the next section to predict the air flow distribution in parallel channels of a PEMFC.

3. Ex-situ and in-situ PEMFC experiments

The entrance region pressure drop method introduced and validated for four parallel tubes in the above sections is applied to measure the instantaneous flow distribution in PEMFC gas flow channels. With this information, it is possible to assess the effects of certain parameters on the distribution of reactants and water products of fuel cell reactions in the channels.

3.1. Ex-situ experimental setup

Ex-situ experiments are designed to study the water transport characteristics in a gas channel by forcing water through a GDL into the gas channels mimicking the actual fuel cell channels. In the present work, eight channels, 0.7 mm wide, 0.4 mm deep and 183 mm long with land widths of 0.5 mm, are employed in parallel. The channel path is weaving with a 5° weaving angle to avoid mechanical shear on the GDL associated with straight channels. The channel dimensions and geometry are based on an actual fuel cell flow design which ensures the best fuel cell performance based on the Department of Energy targets for automotive fuel cells [40]. The header is specially designed to allow the measurement of the pressure drop in the entrance region. Three rows of holes are made in the straight section of the channels to hold the pressure taps, which allow the measurement of the entrance region pressure drop for individual channels. Downstream of the pressure tap holes, another set of holes is drilled to create a provision for dowel pins, which will be used to block all the other channels while calibrating each channel individually. Fig. 6 is a schematic of the header design.

In order to facilitate the measurement of flow distribution in PEMFC parallel channels, an ex-situ experiment is developed [41]. The test section is assembled under compression of 2068 kPa (300 psi), which is equivalent to the clamp pressure normally used in fuel cell stacks. Deionized water (18.2 MΩ, Millipore) is independently delivered to each of the four water chambers through four syringe pumps. However, during the calibration procedure and the dry GDL experiments, no water is injected. Dry clean air generated by a Zero Air Generator (Parker) flows through a bank of rotameters and then into the gas inlet manifold. Fig. 7 shows a schematic for the ex-situ experimental set up.

3.2. Experiments with a plastic sheet

Since the theoretical equations describing the individual channel flow rates as a function of the entrance region pressure drop are not readily available for the specific geometry tested, a calibra-

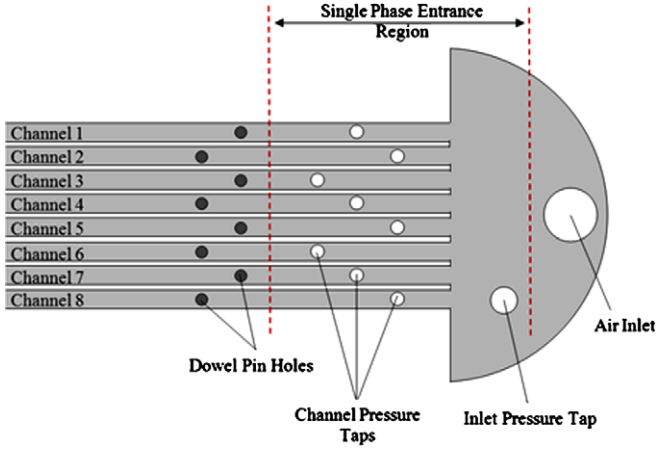

Fig. 6. Header of ex-situ experimental test section including channel pressure tap locations, inlet pressure tap, air inlet, and dowel pin holes. Not to scale.

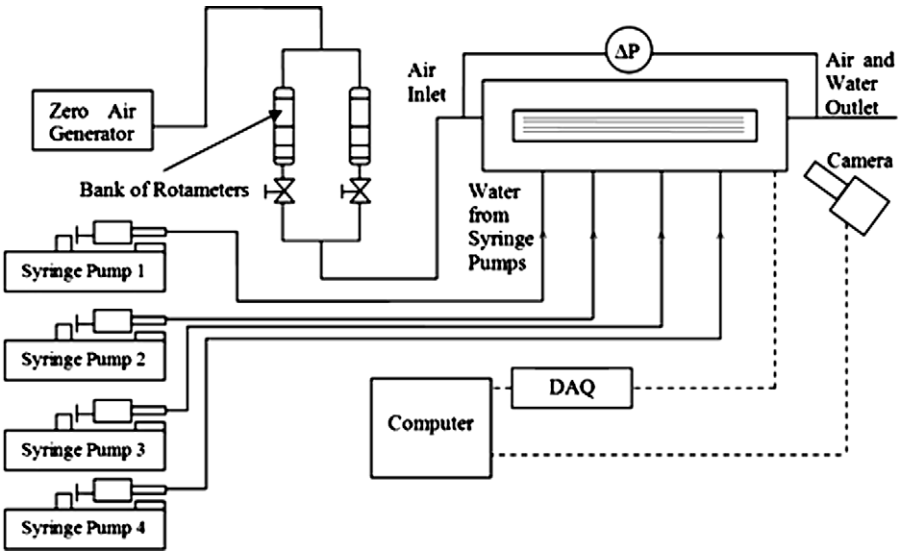

Fig. 7. Schematic of ex-situ experimental setup for simulation of flow maldistribution in a fuel cell. Not to scale.

tion curve is experimentally developed for each channel. A plastic sheet instead of a GDL is used for the calibration since it will allow air flow to be completely blocked off with the use of dowel pins. During the calibration, only the channel of interest is kept open while all other channels are closed using the dowel pins, and air is passed through the channel. The flow rate is measured with a digital flow meter (Omega FMA-1620A), which has an accuracy of ±10 sccm over a range of 0–1000 sccm. The pressure drops in each channel are measured with differential pressure sensors (Honeywell FP2000) and recorded on a computer through a LabVIEW program. This procedure is repeated for each of the eight channels.

Once the calibration procedure is completed, the dowel pins are removed and the holes are carefully sealed leaving all flow channels open. Air with a known flow rate, in the range of 100 to 6000 sccm, is passed through the test section and the entrance region pressure drops in each channel are measured again. Since in this case air flows through all the eight channels, the instantaneous flow rate in individual channel and the flow distribution are obtained from the respective channel calibration curves.

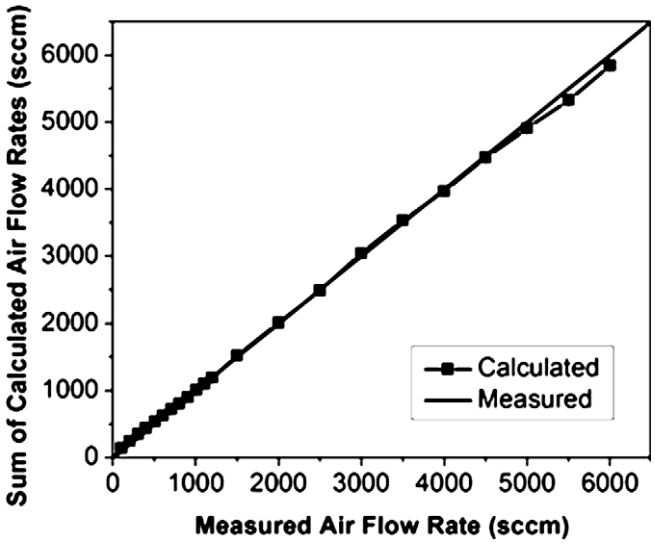

Fig. 8. Comparison of summation of calculated channel flow rates and the measured air flow rates; average of three plastic sheet data used.

3.3. Experiments with GDL

For GDL experiments, the plastic sheet that is used in the earlier experiments is replaced with a GDL material. Three different GDL samples are investigated: a baseline sample which is provided by General Motors, a commercial SGL-25BC sample, and a commercial Toray carbon paper (TGPH-060). Both the baseline and the SGL samples are PTFE treated and have a micro-porous layer (MPL) coating. The thickness of both samples is approximately 250 μm. The Toray TGPH-060 is a PTFE treated but non-MPL coated carbon paper with a thickness of about 190 μm.

For calibration purposes, only air is passed through the channels under dry conditions without any water injection. The total air flow rate in the range of 100 to 6000 sccm is passed through the ex-situ test section and the entrance region pressure drops in each channel are recorded simultaneously. In addition, the total pressure drop across the flow field, i.e., the pressure difference between the inlet and the outlet manifolds, is also measured. This set of experiments provides the flow maldistribution information with single-phase air flow in the flow channels.

In order to identify the flow maldistribution under more realistic two-phase flow conditions in the gas channels, deionized water is injected into the water chambers. Water flows through the GDL under pressure, emerges in the channels and then forms a two-phase flow in the channels. The instantaneous pressure drops in the entrance region for individual channels are recorded. It is worthy to note that the water injection region begins beyond the entrance region pressure taps (see Fig. 6) which guarantees that the pressure measurements are taken in the single phase region and are not interrupted by liquid water. Water injection rates and air flow rates are specially selected to represent the actual water production rates and air flow rates in a real PEMFC with the same flow field design operating steadily at normal operating current densities. In this work, a specific water injection rate of 0.04 mL/min, which corresponds to a current density of 0.4 A/cm^2, is employed. The air flow rate of 400 sccm, corresponding to a stoichiometric ratio of 4, is selected for the present experiments.

A Photron Fastcam-Ultima high-speed camera with an Infinity model K2/S™ long-distance microscope lens is used to capture water formation and the associated two-phase flow patterns inside

the gas channels. Recorded videos had a resolution of 1024 × 1024 and a frame rate range of 60–2000 fps. A dual light guide fiber optic light is used to illuminate the test section. All optical equipment and the test setup are mounted on a vibration isolation table. All the experiments were carried out at ambient temperature and pressure.

4. In-situ experimental setup

An actual operating PEMFC is used to study the effects of electrochemical reactions and two-phase flow on flow maldistribution in gas channels. The test section contains 22 cathode side channels with an active area of 50 cm^2. It also has visual access to visualize the two-phase flow patterns similar to that for the ex-situ setup. The test section design is very similar to the ex-situ design (Fig. 6), except for the current collectors which act as the lands between the channels. The cell was tested using a fuel cell test station (Hydrogenics). The tests were carried out at a cell temperature of 35 °C using dry as well as water saturated hydrogen and air streams. In the future, the cell will be operated at higher temperatures and under different material set and operating conditions.

5. Results and discussion

The entrance region pressure drop technique, established in Section 2 by using water as working fluid, is extended to measure the flow maldistribution in PEMFC parallel channels under both dry and wet conditions.

5.1. Flow distribution with a plastic sheet in ex-situ setup

As described in Section 3.2, channel calibration is first carried out to establish the relationship between the entrance region pressure drop and the gas flow rate through each channel, which is done by passing dry air with a known flow rate through one channel while the other channels are all closed. A plastic sheet instead of a GDL is used during the calibration. The variation of flow rate as a function of the entrance region pressure drop is plotted and a monotonic relation is found between them for the open channel while other channels (blocked) show almost a zero pressure drop. The collected data is fitted with a 5th order polynomial, which is then used as the calibration curve to predict the flow distribution under parallel channel configuration.

In order to test the validity of the calibration equations, a measurement is made where all eight channels are opened and air of a known flow rate is passed through and the pressure drops in each channel are recorded. The flow rate in each channel is calculated from the entrance region pressure drops by using the individual channel calibration equations. The individual channel flow rates are then added and compared with the measured total air flow rate. A small correction factor is then introduced to account for the channel interaction effects (which are seen to be quite small) to further improve the overall agreement. Fig. 8 shows the compar-

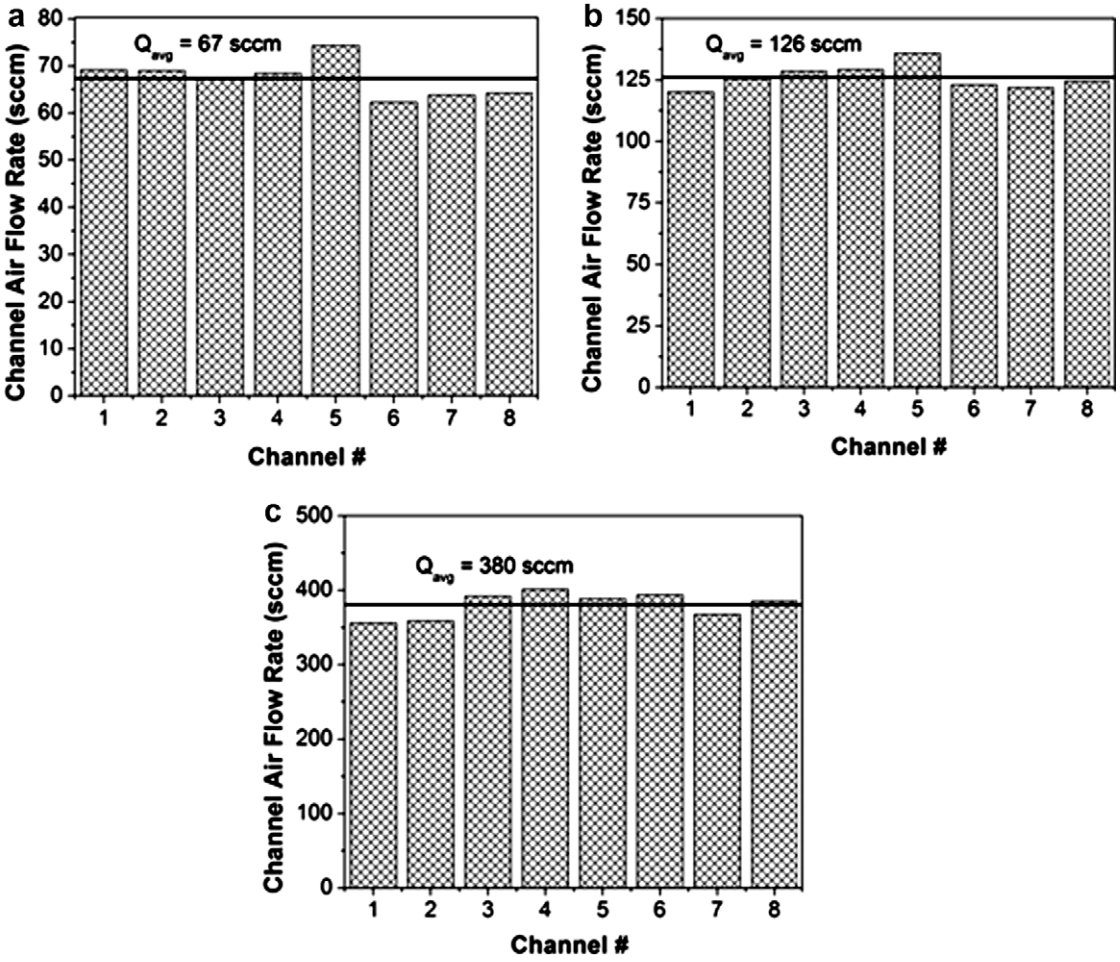

Fig. 9. Flow distribution patterns for plastic sheet and low, medium, and high flow conditions. (a) Flow distribution at an input air flow rate of 300 sccm. (b) Flow distribution at an input air flow rate of 1000 sccm. (c) Flow distribution at an input air flow rate of 3107 sccm.

ison between the summation of calculated channel flow rates and the measured air flow rates. It is seen that the results agree to within 5 percent up to a flow rate of 5000 sccm.

The flow distribution in parallel channels with a plastic sheet is then investigated. Fig. 9a–c shows the predicted flow distribution through each of the channels for three different total flow rates of 500, 1000 and 3100 sccm. It is seen that flow is quite uniform for these cases, except for a slightly higher flow rate in the central channels due to possible manifold effects.

5.2. Flow distribution with dry GDL in ex-situ setup

Similar experiments have been performed on three GDL samples: baseline GDL, SGL-25BC and Toray TGPH-060. For these experiments also, the total measured and predicted flow rates are compared and respective correction factors are obtained for the GDL samples similar to the plastic sheet. The results for the baseline GDL are shown in Fig. 10. Contrary to the plastic sheet case, where the flow is relatively uniform in all the channels, severe flow maldistribution is observed for the baseline GDL at the tested total flow rates. The highest flow rate is found to occur in channel 4 and the lowest in channel 8 for all three total flow rates. A maximum deviation of about 25% is obtained from the mean flow rates at the total flow rates in the range of 300 to 3100 sccm. The possible cause for the maldistribution may be due to different intrusions resulting from the compression effects of the GDL. Flow cross-leakage between adjacent channels, as suggested by Kanezake et al. [37], may also contribute to the maldistribution, but to a lesser degree since parallel channels rather than serpentine flow fields are used here.

The flow distributions with SGL-25BC and Toray TGPH-060 are shown in Fig. 11 (a) and (b), respectively. Severe flow maldistribution is also observed for both GDLs at different total flow rates. The deviations in the individual channel flow rates from the mean flow rate vary from 8% to 16% for SGL-25BC, and from 11% to 27% for Toray TGPH-060 samples respectively in the tested flow rate range. A careful analysis of Figs. 10 and 11 reveals that SGL, Toray and baseline GDLs all show different flow maldistribution patterns. For example, the channel 4 shows the highest flow rate for the baseline GDL case, while the channel 4 and 6 for SGL and Toray sample have almost the same flow rate and are higher than other channels.

5.3. Flow maldistribution during two-phase flow

An important goal of this study is to detect the flow maldistribution caused by the obstructions to reactant flow through PEMFC channels caused by the liquid water blockage. For this purpose, liquid water is injected at the back side of the GDL, simulating the water production in the cathode catalyst layer within a PEMFC. Two-phase flow is thus obtained in the parallel channels and the flow is severely interrupted by the accumulation of water in the channels. Fig. 12 shows the flow distribution and corresponding image of the test section at a water flow rate of 0.04 mL/min and an air flow rate of 400 sccm. As seen from Fig. 12(a), at about 715 s, the flow rate in channel 6 drops sharply. This indicates the

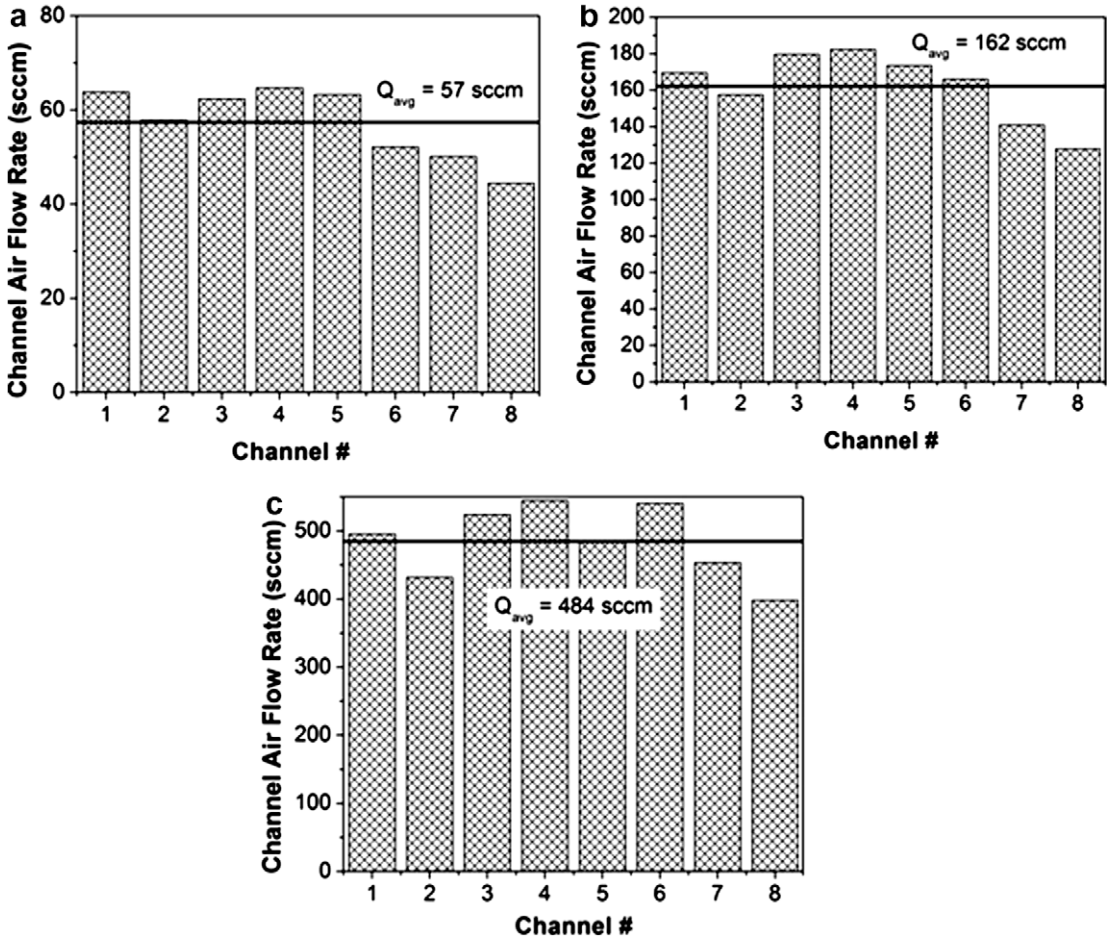

Fig. 10. Flow distribution patterns for the Baseline A sample at low, medium, and high flow conditions. (a) Flow distribution at an input air flow rate of 300 sccm. (b) Flow distribution at an input air flow rate of 1000 sccm. (c) Flow distribution at an input air flow rate of 3107 sccm.

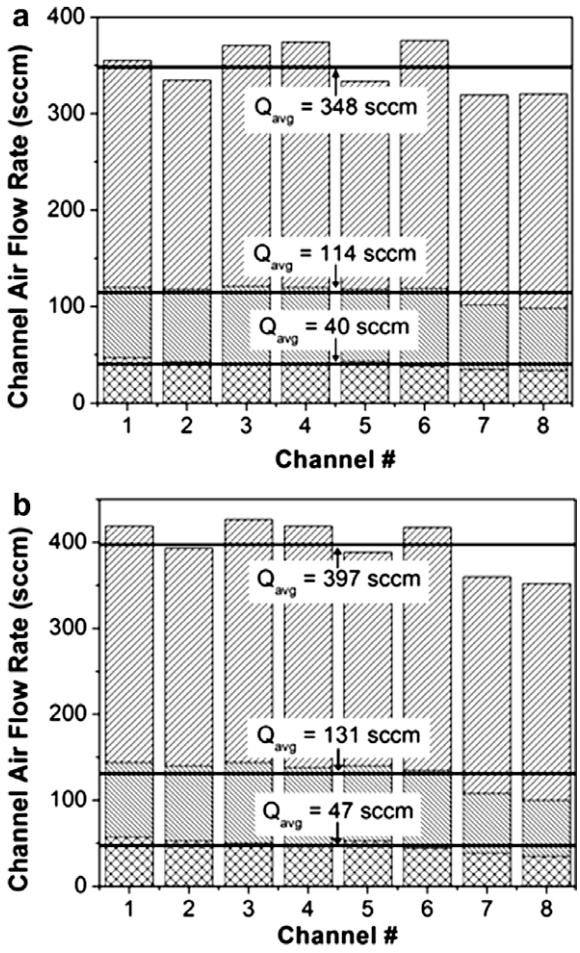

Fig. 11. Flow distribution patterns for the (a) SGL sample and (b) the Toray paper sample. The cross-hatched bars represent the flow rates for 300 sccm input, the diagonal top left to bottom right represent the flow rates for 1000 sccm input, and the diagonal bottom left to top right represent the flow rates for 3107 sccm input.

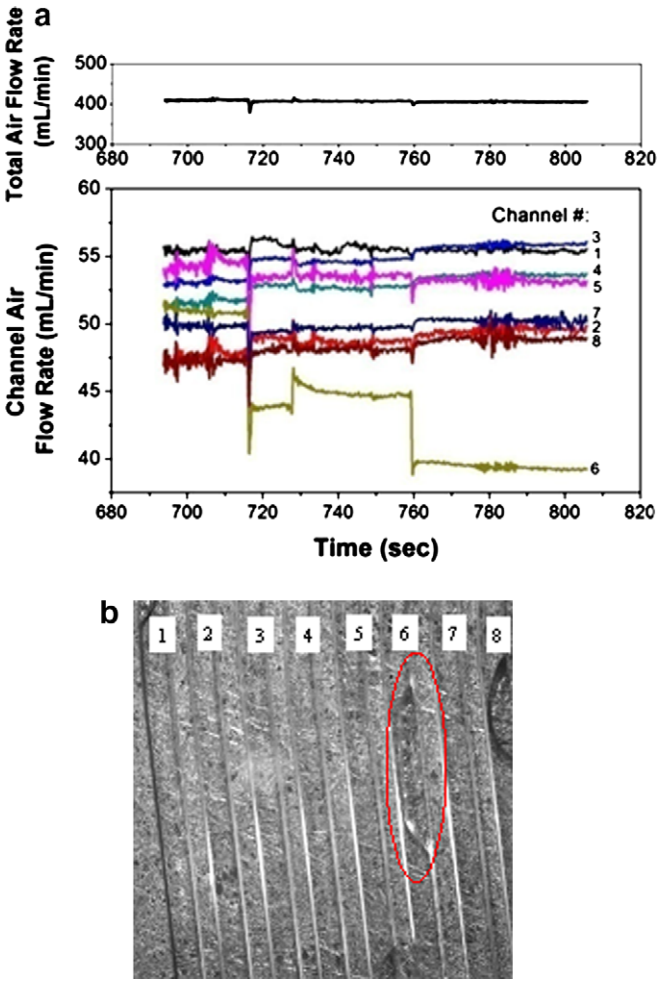

Fig. 12. The ex-situ multi-channel experiment observation, (a) the flow distribution and (b) the flow pattern, at water flow rate of 0.04 mL/min and air flow rate of 400 sccm for the baseline GDL. The numbers in the figures represent the channel number.

formation of a slug in this channel, which is further confirmed by the visual observation obtained from the high-speed image as shown in Fig. 12(b). The flow rates in other channels, channels 1, 3 and 4 in this case, increase to maintain the constant total flow rate. This slug resides in channel 6 for about 15 sec until it is removed by the air flow, reflected by an increase in the air flow rate in channel 6 at 730 s. It may be noted that in Fig. 12(a), the flow rate in channel 6 did not recover to its original value. This may indicate the change of the water flow pattern from the slug to film flow. Due to the strong hydrophilic effect of the channel wall and the corner flow, the slug flow in the gas channel always transforms to a film flow in the later stages of the slug motion. At a time of around 760 s, another slug is formed. It is difficult to identify the location of the new slug because of the limited visual access compared to the entire channel length of 183 mm. This slug resides in the channel until the end of the data recording period. The two-phase flow studies at other air and water flow rates have also been carried out and detailed flow pattern maps will be presented in future publications.

5.4. In-situ flow maldistribution

The flow maldistribution was also measured in an in-situ experimental setup. Fig. 13 shows the flow maldistribution with the dry air at a flow rate of 830 sccm. In this case, only air is passed through the cathode side channels (no hydrogen is passed through the cathode side; therefore there is no electrochemical reaction present) and flow maldistribution is obtained using the same technique as described under the ex-situ testing with GDL. It is noted that flow is not uniform in the channels. The reasons for the maldistribution are: channel dimension non-uniformity, varying local GDL intrusion under compression, and the influence introduced by the specific manifold design. The inlet pipe leading into the inlet manifold entered from the left side. This causes the dynamic head to be higher on the right side channels. In addition, channel dimension non-uniformity and varying local GDL intrusion into the channels are other factors leading to flow maldistribution. Similar flow maldistribution patterns are observed with dry air at other flow rates.

Fig. 14 shows the instantaneous flow maldistribution in the presence of electrochemical reaction. The channel to channel variation needs to be compared with the respective dry case to identify the presence of water in the channels. However careful analysis is warranted because of the cross-communication across the channels. It is seen that the flow distribution is different from the dry case result presented in Fig. 13. For example, the flow in channel #18 is reduced from about 42 sccm in the dry case to about 28 sccm in the wet case. It indicates that there is water present in the channel blocking the flow. The maldistribution in the dry case is caused by the manifold design, and channel dimension reduction due to different GDL intrusion in each channel. In the two-phase case, additional effects due to two-phase flow characteristics in the individual gas channels are

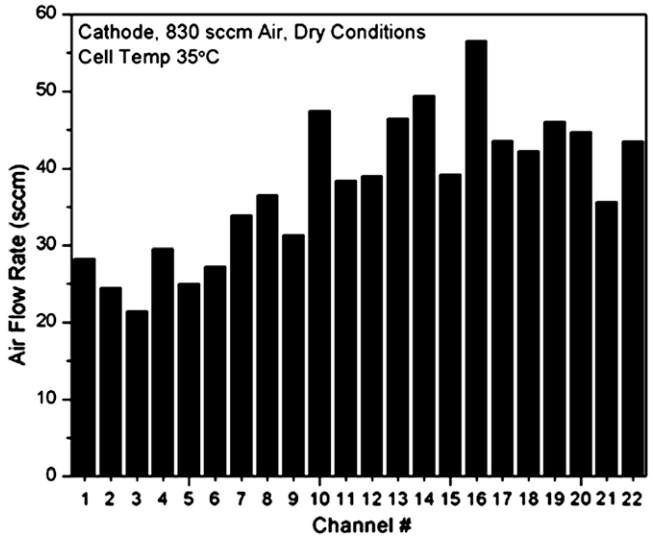

Fig. 13. Flow distribution in individual channels on the cathode side in the in-situ setup without hydrogen (no electrochemical reaction, dry operation), 22 channels, airflow rate 830 sccm.

also present. In studying the effect of water blockage on the fuel cell performance, the reduction in the air flow due to water blockage can be assessed as a function of various system parameters and operating conditions.

The results presented herein are believed to be the first of their kind providing instantaneous flow rate measurements in the gas channels of ex-situ and in-situ fuel cell test setups under both single-phase and two-phase flow conditions. Since the non-uniform flow distribution leads to performance degradation, this study is expected to provide useful insight in the design of flow fields and surface treatment of the GDL and the channel surface.

5.5. Additional notes

These measurements clearly demonstrate the effectiveness of the entrance region pressure drop technique. This technique is readily applicable to channels of any cross-section, and therefore will be useful in many other applications, such as heat exchangers, and other heat and mass transfer devices. If theoretical equations are not available for the desired geometries, individual channel calibration plots may be generated using the same method described in this paper. All channels need not have the same geometry since the calibration plots are generated individually for each channel. However, access to the pressure taps in the entrance region of individual tubes is required to implement this technique and may be a limiting factor in its implementation in operating devices.

The entrance region method can be used to monitor maldistribution resulting from fouling downstream of the entrance region, but cannot be applied if fouling occurs in the entrance region itself. In such a case, an increased pressure drop would not correctly reflect an increased flow rate. If it is known that fouling will occur in the entrance region, but not in the channels themselves, the entrance length method may be modified to measure the pressure drop between a single point in the entrance region and another point downstream in the fully developed region or in the exit header. Appropriate calibration plots must be generated for each configuration. In the future, the experimental data for specific fuel cell geometries may be employed to generate and validate the analytical/numerical models for predicting flow maldistribution for different flow channel configurations, GDL material and operating conditions.

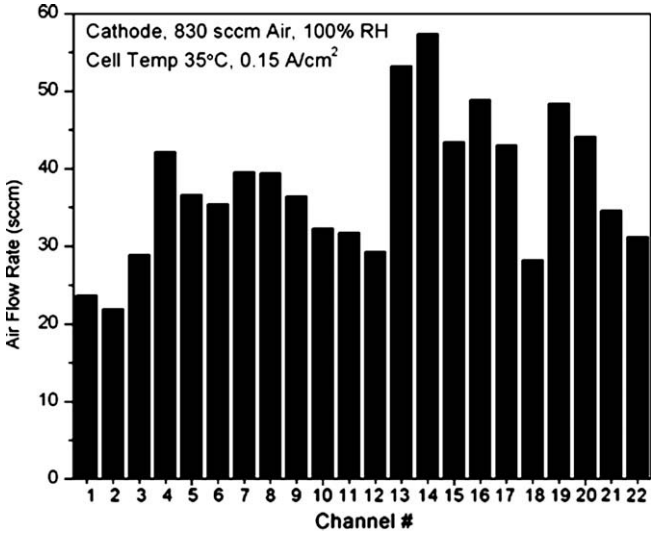

Fig. 14. Flow distribution in individual channels on the cathode side in the in-situ setup with electrochemical reaction, 22 channels, current density of 0.15 A/cm^2, airflow rate 830 sccm.

6. Conclusions

A new technique is proposed to measure the instantaneous flow rate through individual channels in a parallel channel array. Such arrays are used in a number of applications, including fuel cells and heat exchangers. The experimental setup is specifically designed to allow calibration of the individual channel flow rates. The ability of this technique to accurately predict flow maldistribution in parallel channels is experimentally validated in this paper. The method has been implemented in ex-situ and in-situ setups designed to study two-phase flow in gas diffusion channels of a PEMFC to develop effective water management strategies for PEMFCs.

The method is readily applicable to channels of any cross-section and is useful in PEMFC research as shown here. The instantaneous flow rates within a fuel cell can be used to reveal the existing air-water two-phase flow patterns in the gas channels. The method also provides a means to predict and find individual channel obstructions in real time. Understanding and quantifying maldistribution within PEMFC channels is of great importance to the optimization of fuel cell design and performance. The method presented will aid in addressing the concerns related to inefficient usage of the electrochemically active area due to poor water management.

One of the limitations of this technique is the difficulty in accessing the individual channels in the entry region in operating heat transfer devices or fuel cells. However, if implemented in specially designed experimental setups under laboratory conditions, it provides a valuable tool to study maldistribution and its relation with other system parameters.

Further experimentation is needed to define the effectiveness of monitoring only a specific set of channels in an array in order to quantify the overall maldistribution. The application of this method at the fuel cell stack level will prove to be challenging due to the geometry of fuel cell stacks and alterations necessary to implement the method. The experimental stack can be designed to facilitate this measurement, and is planned in the future work.

Acknowledgements

This work was conducted under the project "Visualization of Fuel Cell Water Transport and Performance Characterization under Normal and Freezing Conditions" sponsored by US Department of

Energy grant DE-FG36-07GO17018. The collaborative efforts of Dr. Thomas Trabold and Jon Owejan at the General Motors Fuel Cell Research Center at Honeoye Falls, NY, are gratefully acknowledged.

References

[1] A.C. Mueller, J.P. Chiou, Review of various types of flow maldistribution in heat exchangers, Heat Transfer Engineering 9 (1988) 36–50.
[2] S. Lalot, P. Florent, S.K. Lang, A.E. Bergles, Flow maldistribution in heat exchangers, Applied Thermal Engineering 19 (8) (1999) 847–863.
[3] J.B. Kitto Jr., J.M. Robertson, Effects of maldistribution of flow on heat transfer equipment performance, Heat Transfer Engineering 10 (1) (1989) 18–25.
[4] F.A. Tereda, N. Srihari, B. Sunden, Experimental investigation on port-to-channel flow maldistribution in plate heat exchangers, Heat Transfer Eng. 28 (5) (2007) 435–443.
[5] P.R. Bobbili, B. Sunden, S.K. Das, Thermal analysis of plate condensers in presence of flow maldistribution, Int. J. Heat Mass Transfer 49 (25–26) (2006) 4966–4977.
[6] P.R. Bobbili, B. Sunden, S.K. Das, An experimental investigation of the port flow maldistribution in small and large plate package heat exchangers, Appl. Thermal Eng. 26 (16) (2006) 1919–1926.
[7] Y.Z. Li, J. Wen, A.M. Zhou, K. Zhang, J. Wang, PIV experimental investigation of entrance configuration on flow maldistribution in plate-fin heat exchanger, Cryogenics 46 (1) (2006) 37–48.
[8] B.P. Rao, B. Sunden, S.K. Das, An experimental and theoretical investigation of the effect of flow maldistribution on the thermal performance of plate heat exchangers, J. Heat Transfer Trans. ASME 127 (3) (2005) 332–343.
[9] S. Baek, A. Jiao, Effects of distributor configuration on flow maldistribution in plate-fin heat exchangers, Heat Transfer 26 (4) (2005) 19–25.
[10] B.P. Rao, S.K. Das, An experimental study on the influence of flow maldistribution on the pressure drop across a plate heat exchanger", J Fluids Eng. Trans. ASME 126 (4) (2004) 680–691.
[11] Z. Zhang, Y.Z. Li, Q. Xu, Experimental research on flow maldistribution in plate-fin heat exchangers, Chin. J. Chem. Eng. 12 (1) (2004) 7–13.
[12] A.J. Jiao, Y.Z. Li, C.Z. Chen, R. Zhang, Experimental investigation on fluid flow maldistribution in plate-fin heat exchangers, Heat Transfer Eng. 24 (4) (2003) 25–31.
[13] A.J. Jiao, R. Zhang, S.A. Jeong, Experimental investigation of header configuration on flow maldistribution in plate-fin heat exchanger, Appl. Thermal Eng. 23 (10) (2003) 1235–1246.
[14] M.A.R.S. Al-Baghdadi, H.A.K.S. Al-Janabi, Effect of operating parameters on the hygro-thermal stresses in proton exchange membranes of fuel cells, Int. J. Hydrogen Energy 32 (2007) 4510–4522.
[15] S.D. Knights, K.M. Colbow, J. St-Pierre, D.P. Wilkinson, Aging mechanisms and lifetime of PEFC and DMFC, J. Power Sources 127 (2004) 127–134.
[16] J.P. Meyers, R.M. Darling, Model of carbon corrosion in PEM fuel cells, J. Electrochem. Soc. 153 (2006) A1432–A1442.
[17] S. Dutta, S. Shimpalee, J.W. van Zee, Three-dimensional numerical simulation of straight channel PEM fuel cells, J. Appl. Electrochem. 30 (2000) 135–146.
[18] S. Dutta, S. Shimpalee, J.W. van Zee, Numerical prediction of mass exchange between cathode and anode channels in a PEM fuel cell, Int. J. Heat Mass Transfer 44 (2001) 2029–2042.
[19] T.C. Jen, T. Tan, S.H. Chan, Chemical reacting transport phenomena in a PEM fuel cell, Int. J. Heat Mass Transfer 46 (2003) 4157–4168.
[20] A. Kumar, R.G. Reddy, Effect of channel dimensions and shape in the flow field distributor on the performance of polymer electrolyte membrane fuel cells, J. Power Sources 113 (2003) 11–18.
[21] A. Kumar, R.G. Reddy, Modeling of polymer electrolyte membrane fuel cell with metal foam in the flow field of the bipolar/end plates, J. Power Sources 114 (2003) 54–62.
[22] S.M. Senn, D. Poulikakos, Polymer electrolyte fuel cells with porous materials as fluid distributor and comparisons with traditional channeled systems, J. Heat Transfer Trans. ASME 126 (2004) 410–418.
[23] E. Hontanon, M.J. Escudero, C. Bautista, P.L. Garcia-Ybarra, L. Daza, Optimization of flow-field in polymer electrolyte membrane fuel cells using computational fluid dynamics techniques, J. Power Sources 86 (2000) 363–368.
[24] F. Barreras, A. Lozano, L. Valino, C. Marin, A. Pascau, Flow distribution in a bipolar plate of a proton exchange membrane fuel cell: experiments and numerical simulation studies, J. Power Sources 144 (2005) 54–66.
[25] F. Barreras, A. Lozano, L. Valino, R. Mustata, C. Martin, Fluid dynamics performance of different bipolar plates, part I. velocity and pressure fields, J. Power Sources 175 (2008) 841–850.
[26] S. Um, C.Y. Wang, Three-dimensional analysis of transport and electrochemical reactions in polymer electrolyte fuel cells, J. Power Sources 125 (2004) 40–51.
[27] G. Hu, J. Fan, S. Chen, Y. Liu, K. Cen, Three-dimensional numerical analysis of proton exchange membrane fuel cells (PEMFCs) with conventional and interdigitated flow fields, J. Power Sources 136 (2004) 1–9.
[28] E. Birgersson, M. Vynnycky, A quantitative study of the effect of flow-distributor geometry in the cathode of a PEM fuel cell, J. Power Sources 153 (2006) 76–88.
[29] P. Costamagna, S. Srinivasan, Quantum jumps in the PEMFC science, technology from the 1960s to the year 2000: part II. Engineering, technology development and application aspects, J. Power Sources 102 (2001) (1960) 253–269.
[30] K. Hertwig, L. Martens, R. Harwoth, Mathematical modeling and simulation of polymer electrolyte membrane fuel cells. Part I: model structures and solving an isothermal one-cell model, Fuel Cells 2 (2002) 61–77.
[31] M.B. Ganesh, R. Prabhakar, K.D. Sarit, S. Pandiyan, N. Rajalakshmi, K.S. Dhathathreyan, Analysis of flow maldistribution for fuel and oxidant in a PEMFC, J. Energy Resources Technol. Trans. ASME 126 (2004) 262–270.
[32] A.S. Bansode, S. Patel, T.R. Kumar, B. Muralidhar, Numerical simulation of effects of flow maldistribution on heat and mass transfer in a PEM fuel cell stack, Heat Mass Transfer 43 (2007) 1037–1047.
[33] J.H. Koh, H.K. Seo, C.G. Lee, Y.S. Yoo, H.C. Lim, Pressure and flow distribution in internal gas manifolds of a fuel-cell stack, J. Power Sources 115 (2003) 54–65.
[34] C.-H. Chen, S.-P. Jung, S.-C. Yen, Flow distribution in the manifold of PEM fuel cell stack, J. Power Sources 173 (2007) 249–263.
[35] T.W. Patterson, R.M. Darling, Damage to the cathode catalyst of a PEM fuel cell caused by localized fuel starvation, Electrochem. Solid-State Lett. 9 (2006) A183–A185.
[36] H. Dole, R. Jung, N. Kimiaie, J. Mergel, M. Muler, Interaction between the diffusion layer and the flow filed of polymer electrolyte fuel cells – experiments and simulation studies, J. Power Sources 124 (2003) 371–384.
[37] T. Kanezaki, X. Li, J.J. Baschuk, Cross-leakage flow between adjacent flow channels in PEM fuel cells, J. Power Sources 162 (2006) 415–425.
[38] R.W. Hornbeck, Laminar flow in the entrance region of a pipe, Appl. Sci. Res. 13 (1964) 224–232.
[39] W.M. Kays, A.L. London, Compact Heat Exchangers, McGraw-Hill, New York, NY, 1984.
[40] T. Trabold, J. Owejan, J. Gagliardo, J. Sergi, Two-phase flow considerations in PEMFC design and operation, ICNMM08-62037, Sixth International Conference on Nanochannels, Microchannels and Minichannels, Darmstadt, Germany, June 23–25, 2008.
[41] Z. Lu, A. White, J. Pelaez, M.R. Hardbarger, W. Domigan, J. Sergi, S.G. Kandlikar. Investigation of water transport in an ex-situ experimental facility modeled on an actual doe automotive target compliant fuel cell, ICNMM08-62200, Sixth International Conference on Nanochannels, Microchannels and Minichannels, Darmstadt, Germany, June 23–25, 2008.